Journal of Chromatography A 1670 (2022) 462987

Contents lists available at ScienceDirect

Journal of Chromatography A

journal homepage: www.elsevier.com/locate/chroma

Investigating heparin affinity chromatography for extracellular vesicle purification and fractionation

Benjamin Barnes[a], Thomas Caws[b], Samantha Thomas[b,c], Alex P. Shephard[d], Randolph Corteling[b], Paul Hole[b], Daniel G. Bracewell[a,*]

[a] Department of Biochemical Engineering, University College London, Bernard Katz Building, Gower Street, London WC1E 6BT, UK
[b] ReNeuron, Pencoed Business Park, Pencoed, Bridgend, Mid Glamorgan CF35 5HY, UK
[c] Reproductive Biology and Gynaecological Oncology Group, Institute for Life Science, Medical School, Swansea University, Singleton Park, Swansea SA2 8PP, UK
[d] NanoView Biosciences, Malvern Hills Science Park, Geraldine Road, Malvern WR14 3SZ, UK

ARTICLE INFO

Article history:
Received 25 November 2021
Revised 2 March 2022
Accepted 18 March 2022
Available online 22 March 2022

Keywords:
Extracellular vesicles
Exosomes
Heparin
Purification
Isolation

ABSTRACT

The purification of extracellular vesicles (EVs) remains a major hurdle in the progression of fundamental research and the commercial application of EV-based products. In this study, we evaluated the potential of heparin affinity chromatography (HAC) to purify neural stem cell-derived EVs as part of a multistep process. Bind-elute chromatography, such as HAC, is an attractive method of purification because it is highly scalable, robust and can be automated. Our findings support an interaction between EVs and heparin. The recovery of EVs using HAC based on particle counts was a minimum of 68.7%. We found HAC could remove on average 98.8% and 99.0% of residual protein and DNA respectively. In addition to EV purification, HAC was used to separate EVs into three populations based on their affinity to the heparin column. Within these populations, we detected differences in the expression of the exosome-associated protein TSG101 and the tetraspanin immunophenotype. However, the significance of these observations is not clear. Overall HAC shows promise as a potential purification method to capture EVs and this study proposes a novel application of HAC for EV fractionation. Moving forward, a better understanding of the heparin-EV interaction would be required before HAC can be more widely adopted for these applications.

1. Introduction

Extracellular vesicles (EVs) are rapidly emerging as novel therapeutics and drug delivery platforms. The transition of EV-based products from the laboratory to the clinic requires innovations in process development to drive EV production at scale [1]. A fundamental aspect of this is scalable EV purification that can isolate EVs efficiently and reproducibly.

A variety of methods to purify exosomes have been described, each with their own advantages and disadvantages (Table 1). Ultracentrifugation is frequently used due to its accessibility and detailed evaluation in the literature. However, ultracentrifugation suffers from poor reproducibility due to operator dependence and while it can be scaled using continuous ultracentrifugation, its use in flu vaccine manufacturing being evidence of this [2], achieving the resolution required for EVs will be demanding. These flaws are particularly evident in a commercial setting where scalability and reproducibility are crucial. Alternative EV purification methods based on well-documented techniques, such as size-exclusion chromatography (SEC), have become available that largely overcome these issues but have inherent disadvantages of their own (Table 1). Purification performance can be improved by combining purification methods, for example, ultracentrifugation followed by SEC [3], at the expense of some yield. Purification is improved when combining these methods because EVs are selected based on two criteria, density and size, and ultracentrifugation concentrates the preparation which reduces the size of the SEC column required for processing. Affinity-based methods that target tetraspanins or specific lipids potentially provide superior purification, provided EVs can be eluted without damage [4,5]. However, given the apparent heterogeneity of surface markers expressed on EVs [6], this method will inevitably lead to bias in EV isolation. Furthermore, evaluation of these methods is not always straightforward because selection markers can overlap with the markers used to assess performance.

* Corresponding author.
E-mail address: d.bracewell@ucl.ac.uk (D.G. Bracewell).

https://doi.org/10.1016/j.chroma.2022.462987

Table 1
Commonly used extracellular vesicle (EV) purification methods. [32,33].

Purification method	Advantages	Disadvantages
Ultracentrifugation	■ Well-documented ■ Accessible	■ Potential EV damage ■ Operator dependant ■ Limited scalability for EV applications
Precipitation	■ Relatively easy to implement ■ Scalable ■ Accessible	■ Precipitation agents may need to be verifiably eliminated ■ Limited purification performance
Ultrafiltration	■ Concentration and buffer exchange can be performed in tandem ■ Scalable	■ Shear stress can cause damage to EVs
Anion exchange chromatography	■ Scalable	■ Limited purification performance when used alone
Affinity chromatography	■ High purity achievable through selection of specific proteins or lipids ■ Scalable	■ Selecting for a subset(s) of EVs potentially at the expense of yield
Size-exclusion chromatography	■ Low shear stress	■ Limited scalability and may require a pre-concentration step if used at scale

Heparin is an affinity chromatography ligand used to purify a variety of tag-free proteins and viral particles [7,8]. It is a highly negatively charged glycosaminoglycan and can also act as a cation exchanger [9]. The structure of heparin is related to heparan sulphate proteoglycans (HSPGs) [10], which serve as cell membrane receptors. HSPGs are ubiquitous across cell membranes and are involved in various cellular processes [11–13]. HSPGs are implicated in the uptake of EVs by cells [14]; and heparin has been evaluated as a tool for EV purification [15,16]. Furthermore, the addition of free heparin can inhibit EV uptake [17], although the ligand(s) mediating HSPG binding to EVs have not been identified. However, heparin and heparan sulphate are known to bind to a wide range of ligands many of which could be present on EVs [13].

In this study, we provide evidence to support an affinity between populations of EVs and heparin and we propose two applications of this. Firstly, we demonstrate a chromatography protocol using a linear salt elution gradient which has been designed for EV purification. To assess utility, we compare particle recovery, densitometry-based EV marker recovery, and purity to a commonly used SEC set-up. We demonstrate HAC results in a higher recovery and similar purity of EVs when compared to SEC. Once we established the column provided a reasonable capacity for functional studies based on dose estimates, we focused the remainder of this study on a second application of HAC, EV fractionation. EV fractionation was conducted using a modified HAC protocol, using a step elution gradient, which was run with a larger load volume. EVs were fractionated into two elution fractions and a third flowthrough fraction based on their affinity to heparin. We found differences in the purity and tetraspanin phenotype of EVs in the three fractions. Overall, this study provides insights on this relatively unexplored method of EV capture and advances our understanding of how this can be applied as the field moves towards developing EV-based products.

2. Material and methods

2.1. Cell culture

Human neural stem cells, CTX0E03 cell line (referred to as CTX), were obtained from ReNeuron and cultured as previously described [18]. Cells were grown in T175 flasks to 70% confluency before subculture. Culture media was exchanged every two days. During media exchange, cell culture conditioned media was harvested and clarified by centrifugation at 4000 × g for 20 min at 4°C. Clarified conditioned media (CCM) was stored at 4°C until a minimum of 2 L was accumulated for tangential flow filtration (TFF).

2.2. Tangential flow filtration

Ultrafiltration was performed as described by Gazze et al. [19]. CCM was subjected to TFF using a Spectrum Labs KRIIi Tangential Flow Filtration System fitted with a 100 kDa modified polysulfone hollow fibre module (D02-E100–05-N, Spectrum Labs, Repligen). TFF was operated at a flowrate that ensured shear force was below 2000 s^{-1} and transmembrane pressure was maintained between 1.5 and 3.5 psi. CCM was concentrated 100 times followed by washing with 10 vol of phosphate buffered saline (PBS). Subsequently, the retentate was passed through a 0.22 μm filter and stored at 4°C. The resulting permeate is referred to as TFF material and is used as the chromatography load material throughout this study.

2.3. Heparin affinity chromatography

HAC was performed using 1 mL pre-packed columns (HiTrap Heparin HP, Cytiva Life Sciences). HAC was performed at 1 mL/min with an ÄKTA avant chromatography system (Cytiva Life Sciences). The column was equilibrated with 10 mM sodium phosphate buffer (pH 7). TFF material was diluted (1:3) in 10 mM sodium phosphate buffer (pH 7) and loaded onto the column. Next, the column was washed with 10 mM sodium phosphate buffer (pH 7). Elution was performed using 10 mM sodium phosphate buffer containing 2 M sodium chloride (NaCl).

2.4. Size-exclusion chromatography

SEC was performed using 10 mL gravity-fed columns (qEV original, IZON). 0.5 mL of TFF material was loaded onto each column followed by continuous application of PBS. An initial 2.5 mL fraction was collected as the void volume followed by 1 mL fractions thereafter.

2.5. Absorbence at 280 nm

Absorbence at 280 nm (A280) was continuously recorded during HAC by the ÄKTA avant system (Cytiva). For SEC, A280 of frac-

tions was measured using the NanoDrop 2000c Spectrophotometer (Thermo Fisher Scientific).

2.6. Nanoparticle tracking analysis

Particle size distributions and concentrations were measured using nanoparticle tracking analysis (NTA) with the NanoSight NS300 system (Malvern Panalytical). A syringe pump (Malvern Panalytical) was used to maintain a constant sample flowrate. Samples were diluted in PBS until an average of 30 to 80 particles per frame were recorded. Particles were tracked over three 120 s periods per measurement and an average was taken. All measurements were taken with the camera level set to 16, a detection threshold of 5 and with blur size and max jump distance set at auto. 100 nm polystyrene spheres (Malvern Panalytical) were run prior to each set of sample measurements to confirm the accuracy of the sizing.

2.7. Gel electrophoresis and western blotting

Lithium dodecyl sulphate sample buffer (NuPAGE, Invitrogen) was added to samples in a 1:3 vol ratio and heated at 70°C for 10 min. Dithiothreitol reducing agent was added if appropriate (NuPage, Invitrogen). Samples were separated by SDS-PAGE on precast 4 to 12% Bis-Tris protein gels (NuPAGE, Invitrogen) and transferred onto polyvinylidene difluoride membranes (0.45 µm, Invitrogen). Membranes were blocked for 1 h at room temperature according to manufacturer guidelines (Invitrogen WesternBreeze Blocker/Diluent Part A and B). Membranes were incubated with primary antibodies at 4°C overnight. The following primary antibodies were used: mouse anti-human calnexin (1:100, Invitrogen MA3–027), mouse anti-human serum albumin (HSA) (1:100, Invitrogen MA1–20,124), rabbit anti-human TSG (1:400, Abcam ab125011), mouse anti-human CD81 (1:100, Invitrogen 10630D), mouse anti-human CD63 (1:100, Invitrogen 10628D) and, mouse anti-human CD9 (1:100, Invitrogen 10626D). After washing (Invitrogen WesternBreeze Wash Solution), membranes were incubated with goat anti-mouse horseradish peroxidase conjugate (1:500, Invitrogen 31,430) or donkey anti-rabbit horseradish peroxidase conjugate (1:500, Abcam ab205718) as appropriate. Protein bands were detected using a charge-coupled device imager (Amersham Imager 600, Cytiva Life Sciences) after a five-minute incubation with enhanced chemiluminescent substrate (Invitrogen SuperSignal West Femto Maximum Sensitivity Substrate, Thermo Fisher Scientific). Densitometry analysis was conducted using ImageQuant TL (Cyiva Life Sciences).

2.8. Bicinchoninic acid assay

Protein concentrations were determined using a bicinchoninic acid (BCA) assay kit (Thermo Fisher Scientific 23,235) in 96-well plates following manufacturer guidelines. The absorbence at 562 nm was measured using the CLARIOstar Plus (BMG Labtech).

2.9. DNA quantification assay

Double-stranded DNA (dsDNA) concentrations were measured using the PicoGreen dsDNA quantification assay (Thermo Fisher Scientific P7589) in 96-well plates following manufacturer guidelines. Fluorescence was detected using the CLARIOstar Plus (BMG Labtech).

2.10. ELISA-like assay

EV makers were detected using an enzyme-linked immunosorbent assay-like (ELISA-like) assay. TFF material and chromatography samples were incubated in high-binding 96-well plates at 4°C overnight (Greiner 756,071). A volume equivalent to 1 µg of protein was loaded per well (triplicates were run for each sample/marker combination). All subsequent incubations were untaken on a rocker at room temperature and in between every incubation step, wells were washed with PBS three times. Wells were blocked with 1% (w/v) bovine serum albumin for 2 h before incubation with the following mouse anti-human primary antibodies and isotype controls at a 1:1000 dilution: Alix (SantaCruz SC-166,952), TSG101 (SantaCruz SC-7964), CD81 (Bio-Rad MCA1847EL), CD63 (BioRad MCA2142), CD9 (R&D Biosystems MAB1880), IgG1 (eBioscience 14–4714–85), IgG2A (eBioscience 14–4724–85) and IgG2B (eBioscience 14–4732–85). Samples were incubated with goat anti-mouse biotin-labelled secondary antibody (1:1000, Perkin Elmer NEF823001EA) for 1 h. Next, samples were incubated with europium-labelled streptavidin (Perkin Elmer 1244–360) diluted in Buffer Solution RED (1:1000, Kaivogen 042–02) for 45 min. Finally, samples were incubated with Europium Fluorescent Intensifier (Kaivogen 042–04) for 5 min before time-resolved fluorescence energy transfer (340 nm excitation/665 nm emission) was measured using the CLARIOstar Plus (BMG Labtech) [19–22].

2.11. Transmission electron microscopy

EVs were visualised using transmission electron microscopy (TEM). 1 µL of undiluted TFF material and chromatography samples were incubated on each formvar-carbon grid for two minutes. Grids were gently drained between all incubation steps. Subsquently, grids were placed on droplets of PBS for 30 s and stained on droplets of 1% uranyl acetate (w/v) for 30 s. The grids were then drained and allowed to dry before observation using a Jeol1010 transmission electron microscope. Images were captured with a Gatan Orius camera.

2.12. ExoView

Samples were analysed using the ExoView Human Tetraspanin Kit (NanoView Biosciences). Samples were diluted in manufacturer supplied buffer, solution A, and incubated overnight at room temperature on ExoView Tetraspanin Chips. Chips were washed three times in solution A, prior to incubation with fluorescent tetraspanin antibodies. Labelling antibodies consisted of anti-CD9 (CF488), anti-CD81 (CF555) and anti-CD63 (CF647). Antibodies were diluted 1:500 as per manufacturer's instructions and incubated on chips for 1 h at room temperature. Chips were then washed in kit supplied buffers, dried and imaged by the ExoView R100 using nScan v2.9.5. Data were analysed using NanoViewer 2.9.5. Fluorescent cut-offs were set relative to the monoclonal IgG control.

2.13. Purity

The purity of EVs was calculated using the following formula:

$$\text{Purity (particles/µg of protein)} = \frac{C_{Particle} \times V}{C_{Protein} \times V} \quad \text{(Eq. 1)}$$

where $C_{Particle}$ is the concentration of particles (particles/mL), $C_{Protein}$ is the concentration of total protein (µg/mL) and V is the fraction volumes (mL).

2.14. Log removal

The log removal (LRV) of particles, protein and dsDNA was calculated as follows:

$$\text{Log removal} = \log_{10}(B/A) \quad \text{(Eq. 2)}$$

where A and B are the amounts of particles, protein and dsDNA before and after the chromatography step, respectively.

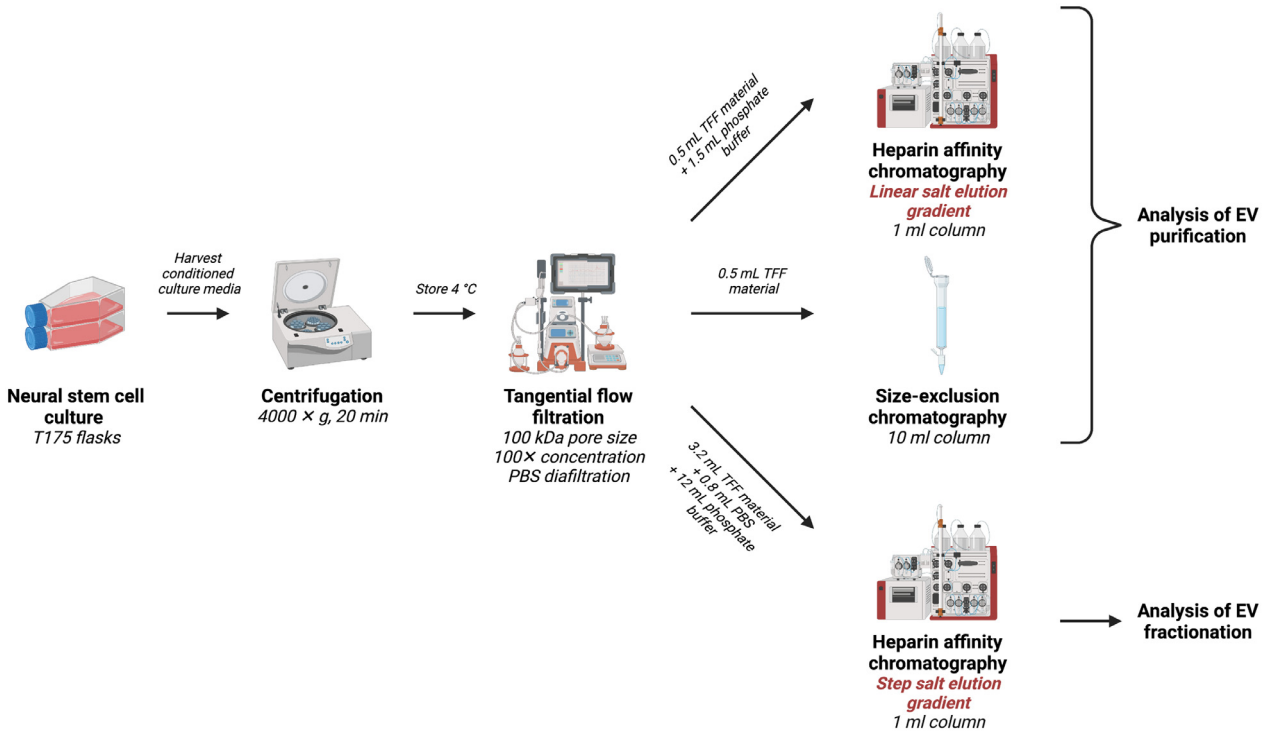

Fig. 1. Experimental overview. This study describes two main sets of experiments. Firstly, we compared heparin affinity chromatography (HAC), using a linear elution gradient, to size-exclusion chromatography to assess the potential of HAC to capture extracellular vesicles (EVs). Secondly, we replaced the linear elution gradient with a step gradient in the HAC protocol and evaluated the purification performance and ability to fractionate EVs. TFF: tangential flow filtration material. Illustration created with BioRender.com.

3. Results

3.1. EV elution using a linear salt gradient

Prior to chromatography, TFF is used for the primary recovery of EVs from CCM and serves as an initial purification step, removing impurities with molecular weights less than 100 kDa. The retentate is concentrated by a factor of 100, washed with PBS and filtered through a 0.22 µm filter. Therefore, the resulting TFF material is highly concentrated and of a narrow size range.

To evaluate the potential of HAC to isolate EVs, a NaCl linear elution gradient was initially used and compared to a general SEC protocol (Fig. 1). 0.5 mL of TFF material was loaded into each column. Five fractions from the heparin column (H1–H5) and four fractions from the size-exclusion column (S1–S4) were collected for NTA and western blot analysis.

Protein content was monitored in each fraction using A280. For HAC, a large initial A280 peak was observed indicating the presence of species that do not bind to the column in the flowthrough (Fig. 2a). Application of the salt gradient during the elution stage released bound species from the column resulting in a smaller broad A280 peak. Particle concentrations in fractions corresponding to the elution peak (H2–H4) were higher than fraction H1 which corresponded to the flowthrough (Fig. 2b). H3 had the highest particle concentration of 3.62×10^{10} particles/mL. Particle modal size was between 60.7 and 65.1 nm in elution fractions with no major differences in particle modal size seen across all fractions (Fig. 2c). Associated size distributions are shown in the appendix (Fig. A1). H3 had the highest number of total particles at 3.62×10^{10}. Elution fractions H2–H4 had a total of 8.45×10^{10} particles (Fig. 2d). Particle recovery was calculated as an indication of EV recovery (Fig. 2e). Elution fractions accounted for 68.7% of particles loaded onto the column (fractions H2–H4). However, fractions H2–H4 only make up 3 mL out of the 5 mL elution peak. Therefore, we expect particle recovery in the entire elution peak to be higher. The purity of fractions H2–H4 ranged from 3.49×10^8 to 9.46×10^8 particles/µg of protein (Fig. 2f). The purity of fraction H5 was the highest at 4.68×10^9 particles/µg of protein. However, western blot analysis revealed no EV markers were present in H5. This indicates that these particles are not EVs. We saw an enrichment of EV markers, CD9, CD63 and CD81, in elution fractions H2–H4. The presence of HSA, a known process impurity found in the culture medium, in flowthrough fraction H1 was comparable to the TFF material which was loaded onto the column. Conversely, lower HSA levels were seen in elution fractions H2–H4 (Fig. 2g). Densitometry analysis was conducted on western blots. Pixel counts were volume-adjusted and compared to TFF material to give a broad estimate of pixel recovery for each marker (Fig. 2h). Volume-adjusted pixel counts are shown in the appendix (Fig. A3a). For tetraspanin markers, CD9, CD63 and CD81, the average recovery was 26.4% with a standard deviation of 12.9%. The recovery of HSA in flowthrough fraction H1 was 60.0%, indicating removal of HSA.

For SEC, we pooled the first 2.5 mL (S1) and collected the next three 1 mL fractions for EV analysis (S2–S4). An initial A280 peak was observed which corresponded to fractions S2–S4 followed by a larger A280 peak (Fig. 3a). NTA particle concentration peaked at 2.95×10^{10} particles/mL in S3 (Fig. 3b). Particle modal size decreased from 107.8 to 57.3 nm across S2–S4 indicating SEC is separating species by size (Fig. 3c). Size distributions are shown in Fig. A1 (appendix). S3 contained the highest number of particles at 2.95×10^{10} (Fig. 3d). Particle recovery was 39.8% in elution fractions S2–S4 (Fig. 3e). The purity of S2–S4 ranged from 2.72×10^8 to 8.64×10^8 particles/µg of protein (Fig. 3f). Western blot analysis detected an enrichment of EV markers, CD9, CD63 and CD81, in S2–S4 with S3 displaying the greatest enrichment. Furthermore, the HSA signal increased across S2–S4 supporting the

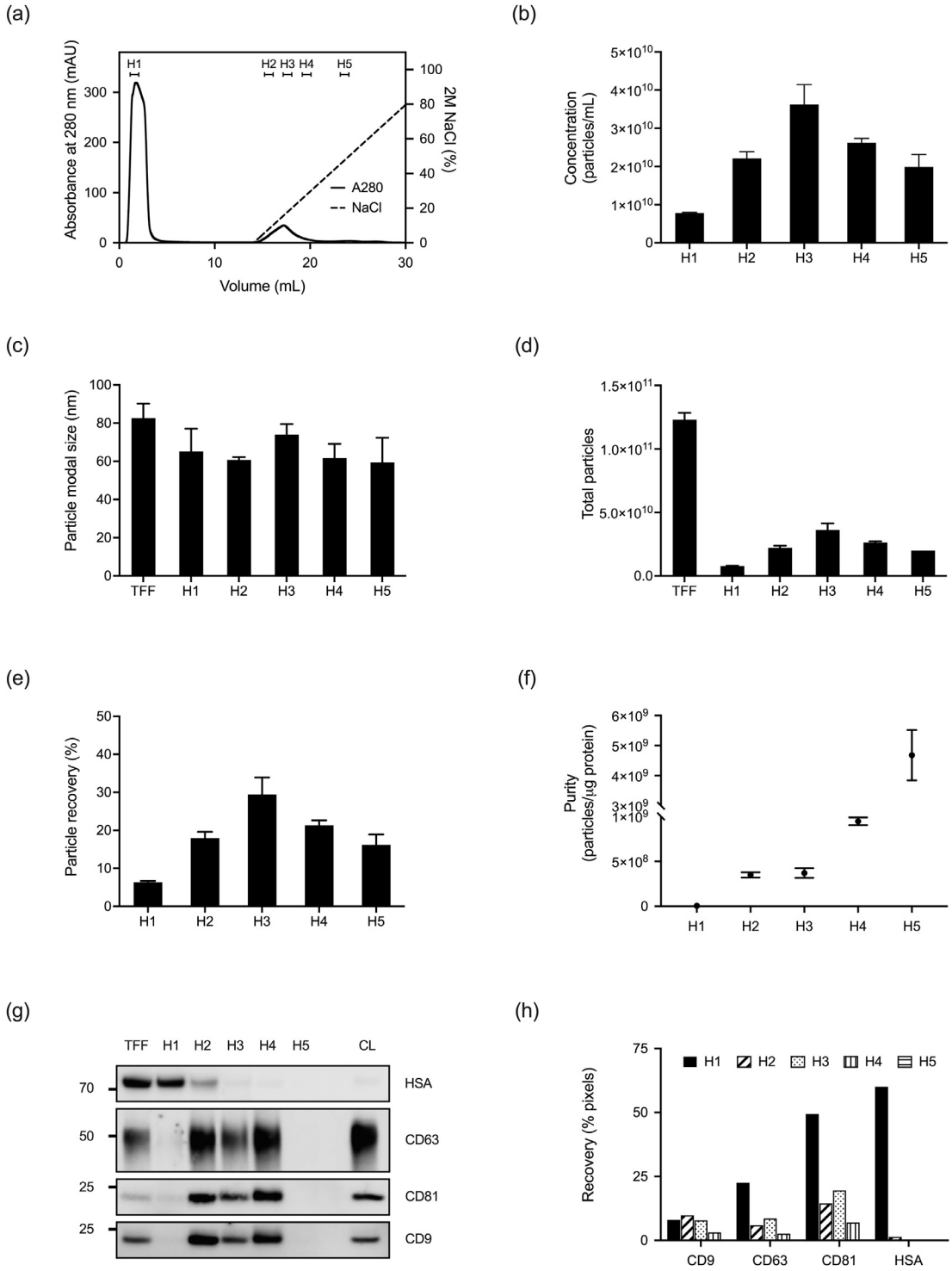

Fig. 2. Heparin affinity chromatography (HAC) using a linear elution gradient. 0.5 mL of tangential flow filtration material (TFF) was diluted in 1.5 mL of 10 mM sodium phosphate buffer (pH 7) before being loaded onto a 1 mL column. 1 mL fractions were collected. (a) Absorbance at 280 nm (A280) and elution buffer concentration for HAC. (b) Nanoparticle tracking analysis (NTA) particle concentrations. (c) NTA particle modal size. (d) NTA total particle counts. (e) NTA particle recovery. (f) Purity. (g) Western blot analysis of HAC fractions showing tetraspanin EV markers and impurity marker, human serum albumin (HSA). 0.45 µg of protein was loaded per lane. (h) Recovery based on densitometry analysis of western blots. Error bars represent the standard deviation of technical repeats ($n = 3$). NaCl: sodium chloride; H1–H5: HAC fractions 1–5; CL: CTX cell lysate.

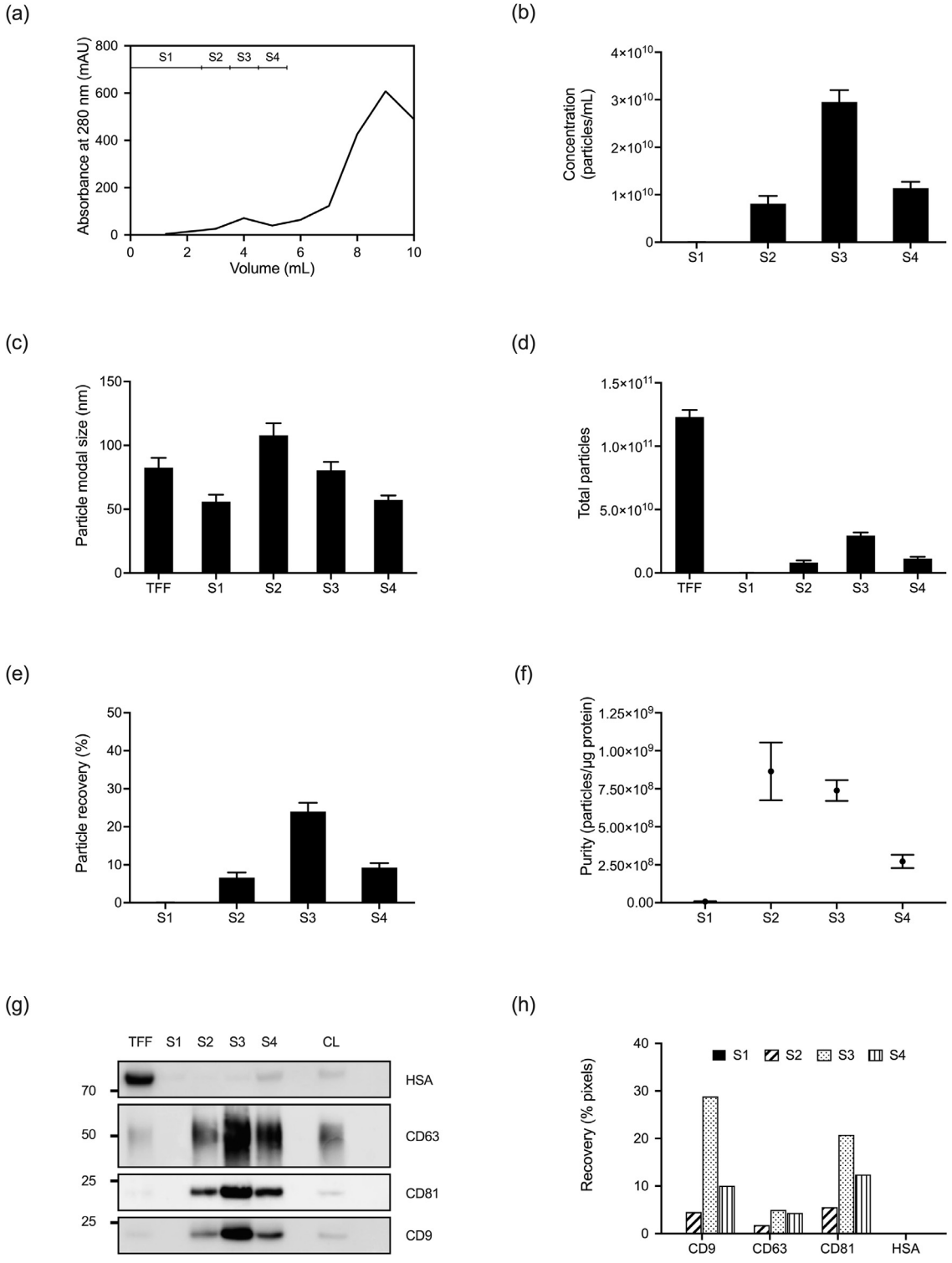

Fig. 3. Size-exclusion chromatography (SEC). 0.5 mL of tangential flow filtration material (TFF) was loaded onto a 10 mL column. After an initial 2.5 ml fraction was collected, 1 mL fractions were collected thereafter. (a) Absorbance at 280 nm (A280). (b) Nanoparticle tracking analysis (NTA) particle concentrations. (c) NTA particle modal size. (d) NTA total particle counts. (e) NTA particle recovery. (f) Purity. (g) Western blot analysis of SEC fractions showing tetraspanin EV markers and impurity marker, human serum albumin (HSA). 0.45 µg of protein was loaded per lane. (h) Recovery based on densitometry analysis of western blots. Error bars represent the standard deviation of technical repeats ($n = 3$). S1–S4: SEC fractions 1–4; CL: CTX cell lysate.

Table 2
Mass balances for particles, residual host protein and double-stranded DNA (dsDNA).

	Volume (mL)	Particles (10^8 particles/mL)	Particle Recovery (%)	Total Protein (µg/mL)	Total Protein Recovery (%)	dsDNA (ng/mL)	dsDNA Recovery (%)
TFF	3.2	618 ± 14.1	N/A	1630 ± 71.4	N/A	382 ± 16.1	N/A
FT	17.5	70.0 ± 6.42	62.0 ± 5.86	213 ± 15.5	71.4 ± 6.06	48.0 ± 1.39	68.8 ± 3.52
WASH	7.5	4.82±0.248	1.83 ± 0.103	2.90 ± 0.501	0.417 ± 0.0742	1.01 ± 0.184	0.621 ± 0.116
E1	1	125 ± 10.7	6.31 ± 0.562	59.6 ± 0.844	1.14 ± 0.0523	7.07 ± 0.00	0.578 ± 0.0244
E2	2	140 ± 11.7	14.1 ± 1.23	31.0 ± 0.297	1.18 ± 0.0529	9.08 ± 0.145	1.49 ± 0.0671
Total			**83.2**		**74.1**		**71.4**

3.2 mL of tangential flow filtration material (TFF) was topped up to 4 mL with phosphate buffered saline and diluted in 12 mL of 10 mM sodium phosphate buffer (pH 7) before being loaded onto the column. FT: heparin affinity chromatography (HAC) flowthrough; WASH: HAC wash; E1: HAC elution fraction 1; E2: HAC elution fraction 2.

expectation of smaller impurities eluting from the column after EVs (Fig. 3g). Densitometry-based recovery for tetraspanin markers was 31.1% with a standard deviation of 17.5% (Fig. 3h). Fig. A3b shows volume-adjusted pixel counts. The recovery of HSA was negligible across all the tested fractions. Due to the small size of HSA, we expect it would have eluted from the column at a later stage.

In summary, A280 was lower and particle concentrations higher in elution fractions, H2–H4 and S2–S4 for HAC and SEC respectively. An enrichment of EV markers and a reduction in HSA was seen in elution fractions relative to the TFF material (column load material). Particle recovery in elution fractions was at least 68.7% using HAC and 39.8% using SEC. These initial experiments suggest that heparin columns bind EVs. Therefore, HAC shows potential as an EV purification method and has the advantage of being more scalable than methods such as ultracentrifugation and SEC. During these experiments, we also noted that the elution peak seen in Fig. 2a was broad, which we hypothesised resulted from mulitiple species being eluted.

3.2. HAC elution using a step salt gradient

Based on the broadness of the elution peak in Fig. 2a, we sought to separate out this peak further using a step NaCl elution gradient (Fig. 4). We anticipated the elution peak was formed from the elution of multiple species which could potentially be different EV subpopulations with varying degrees of affinity to heparin. Consequently, we increased the volume of TFF material loaded onto the column to 3.2 mL to saturate the column and increase the concentration of EVs in elution fractions to aid analysis, at the expense of EV recovery. The flowthrough produced an initial large A280 peak (FT in Fig. 4a). Two A280 elution peaks were observed at 0.2 M and 0.4 M NaCl (E1 and E2 respectively).

3.2.1. Particles, protein and DNA mass balances

To assess the usefulness of HAC to remove impurities we measured particle counts, residual protein and residual dsDNA concentrations. Particle concentrations were higher in E1 and E2 compared to FT (Fig. 4b). Particle modal size was broadly consistent across all fractions between 88.3 to 111.0 nm (Fig. 4c). Associated size distributions are shown in Fig. A2 (appendix). Fractions E1 and E2 collectively contained 4.04×10^{10} particles representing a recovery of 20.4% (Fig. 4d). Fig. 4e shows the log removal of the particles and the two types of impurity: protein and dsDNA. We expect particles to be made up of EVs in addition to other species such as proteins aggregates. 1.20 and 0.850 LRVs of particles, 1.94 and 1.93 LRVs of protein, and 2.24 and 1.83 LRVs of dsDNA were removed from E1 and E2 respectively. Table 2 shows the impurity mass balances. 83.2%, 74.1% and 71.4% of particles, protein and dsDNA respectively, were accounted for in the fractions collected. The majority of remaining particles, protein and dsDNA are likely to have been eluted at 2 M NaCl (Fig. 4a) or remained bound to the column, and therefore were not collected. Purity rose from 0.378×10^8 particles/µg of protein in TFF material to 2.09×10^8 and 4.51×10^8 particles/µg of protein in E1 and E2 respectively (Fig. 4f). ExoView-based particle data was also used to calculate purity (Fig. A4 in the appendix). The trend in ExoView-based purity matches NTA-based purity. We found ExoView based purity was greater than NTA-based purity with fractions E1 and E2 having purities of $1.46–1.95 \times 10^9$ and $1.91–2.70 \times 10^9$ particles/µg of protein, respectively. At the time of writing, the ExoView platform does not provide a particle concentration calculation. While this function is being integrated, dilution-adjusted particle counts were multiplied by a factor of 50,000 to calculate particles per mL, as instructed by NanoView Biosciences. Based on this approach, we expect ExoView-based purity offers a broad estimate. This could account for ExoView-based purity exceeding NTA-based purity, which is unexpected considering only particles positive for particular markers are counted.

3.2.2. EV and impurity markers

Western blot analysis was used to probe for external EV markers, CD9, CD63, CD81, internal marker TSG101 and impurity markers HSA and calnexin (Fig. 5a). CD9, CD63 and CD81 were detected in all fractions but were enriched in elution fractions E1 and E2. The presence of tetraspanins in the FT fraction was low relative to total protein. TSG101 was detected in E2. However, only very faint TSG101 bands can be seen in other fractions. The process impurity HSA was detected in all fractions. HSA is supplemented into the CTX culture media and is expected to be present at relatively high levels in CCM. HSA was detected at lower levels in elution fractions, with E2 showing the faintest band. The endoplasmic reticulum-associated marker, calnexin, was used as a second impurity marker. As expected, calnexin was only detectable in the cell lysate. Densitometry-based recovery of tetraspanin markers and TSG101 was 15.4% and 10.0% respectively in E1 and E2 collectively (Fig. 5b). HSA recovery in FT was 60.7%, which is close to the 60.0% found in flowthrough fraction H1 in the linear gradient elution protocol (Fig. 2h). Associated volume-adjusted pixel counts are shown in Fig. A3c (appendix). Western blots were reinforced by the ELISA data (Fig. 5c) which showed a similar trend in tetraspanin presence across the four samples. There were significant differences in the relative fluorescence of all tetraspanin markers between elution fractions E1 and E2. Samples are not lysed during the ELISA protocol and therefore internal EV markers are not detectable in intact EV preparations. As expected Alix and TSG101 were not detected in any sample by ELISA, which may suggest EVs retained their integrity during HAC.

3.2.3. Visualisation of vesicles

Undiluted samples were negatively stained using 1% uranyl acetate (w/v) and visualised using TEM. Close-up and wide-field representations are shown in Fig. 6. The highest vesicle density was observed in TFF material. As expected, these vesicles were surrounded by a large area of aggregated protein. Conversely, the FT fraction exhibited the lowest vesicle density, but similar levels of

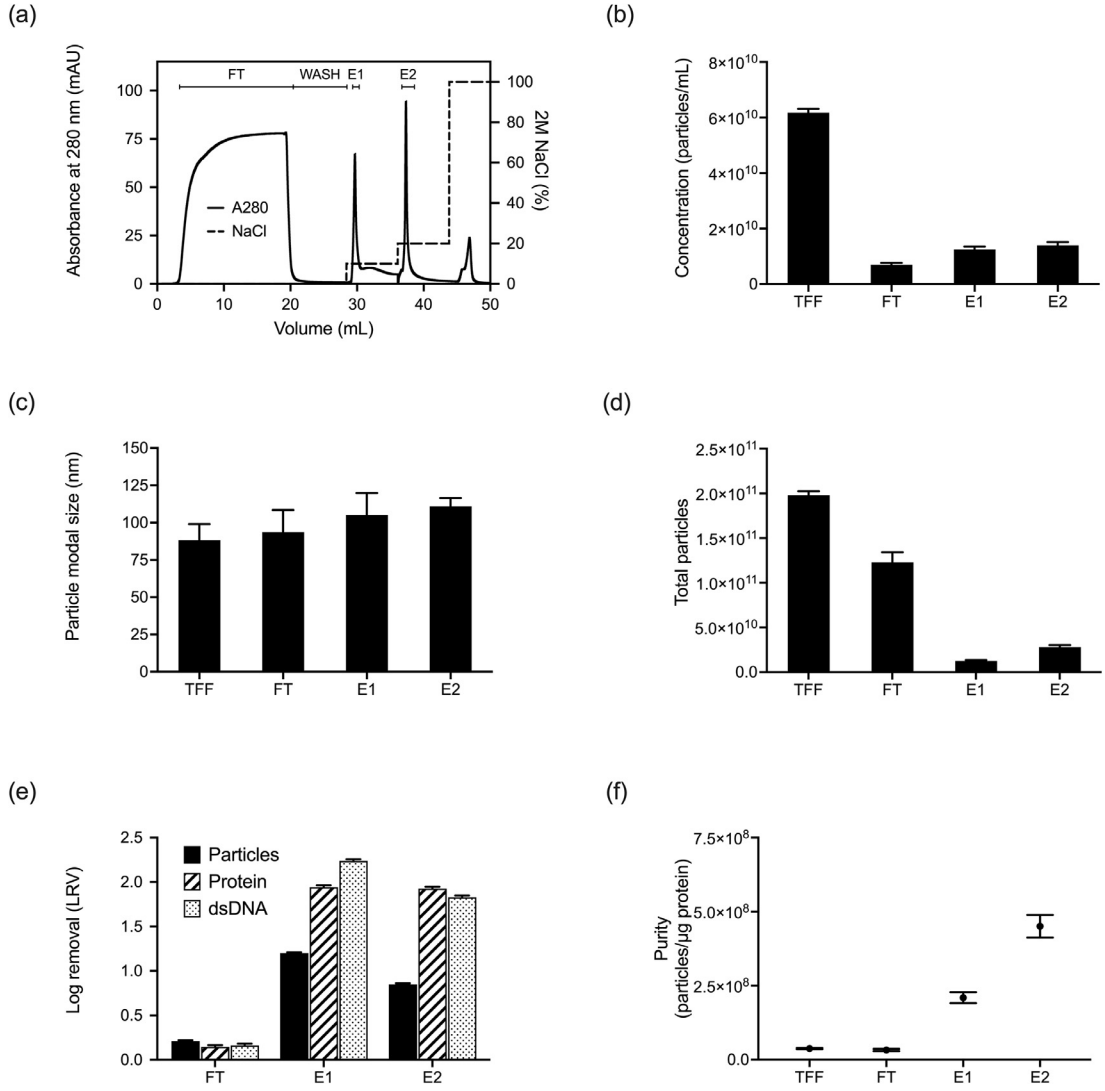

Fig. 4. Heparin affinity chromatography (HAC) using a step elution gradient and associated particle, residual host cell protein and double-stranded DNA (dsDNA) analysis. 3.2 mL of tangential flow filtration material (TFF) was topped up to 4 mL with phosphate buffered saline and then diluted in 12 mL of 10 mM sodium phosphate buffer (pH 7). 0.5 mL fractions were collected and pooled where appropriate into four categories: flowthrough (FT), wash (WASH), elution fraction 1 (E1) and elution fraction 2 (E2) (see Table 2 for volumes of each category). (a) Absorbance at 280 nm (A280) and elution buffer concentration. (b) Nanoparticle tracking analysis particle (NTA) concentrations. (c) NTA particle modal size. (d) NTA total particle counts. (e) Log removal of particles, protein and dsDNA. (f) Purity. Error bars represent the standard deviation of technical repeats ($n = 3$). NaCl: sodium chloride.

aggregated protein were observed. The trend in observed aggregated protein in micrographs corresponded well with protein concentrations determined using the BCA assay (Table 2). Vesicular structures (concave discs) were observed in E1 and E2. Whereas the observed aggregated protein was relatively low in both elution fractions.

3.2.4. EV tetraspanin phenotype analysis

Building on the identification of EVs in both elution peaks, we used the ExoView platform to explore whether HAC was fractionating EVs into populations with differing tetraspanin expression by determining whether: 1) specific tetraspanin-positive vesicles were more prevalent in certain fractions; 2) the tetraspanin phenotype changed between elution fractions. The ExoView platform works by capturing EVs using antibodies against specific EV membrane proteins. Once captured, EVs can be sized and incubated with fluorescent probes against external EV markers. Here, we captured and probed using CD9, CD63 and CD81 (Fig. 7a). The size distribution for particles expressing CD9, CD63 and CD81 are shown in Fig. 7b–e. Size distributions ranged from around 50 to 100 nm for all samples which is consistent with expected small EV sizes [23].

Total particle counts are quantified in Fig. 7f. Differences in the number of marker-positive particles were seen within fractions. To illustrate this, the number of CD81-positive particles was significantly higher than both CD9- and CD63-positive particles in TFF material. Whereas, this same trend is not seen in elution fractions where CD81-positive particles are not significantly more abundant than CD9-positive particles. CD63-positive particles were the least abundant in elution fractions. Particle counts are broadly proportionate to particle concentration, and we can see the trend in total particle counts across the four samples is consistent with NTA data (Table 2). We expect the presence of EVs in the FT resulted from the saturation of the column due to increased load volume and from EVs that do not bind to heparin.

Colocalisation analysis was performed to explore the tetraspanin phenotype between samples (Fig. 7g–i). CD9-captured

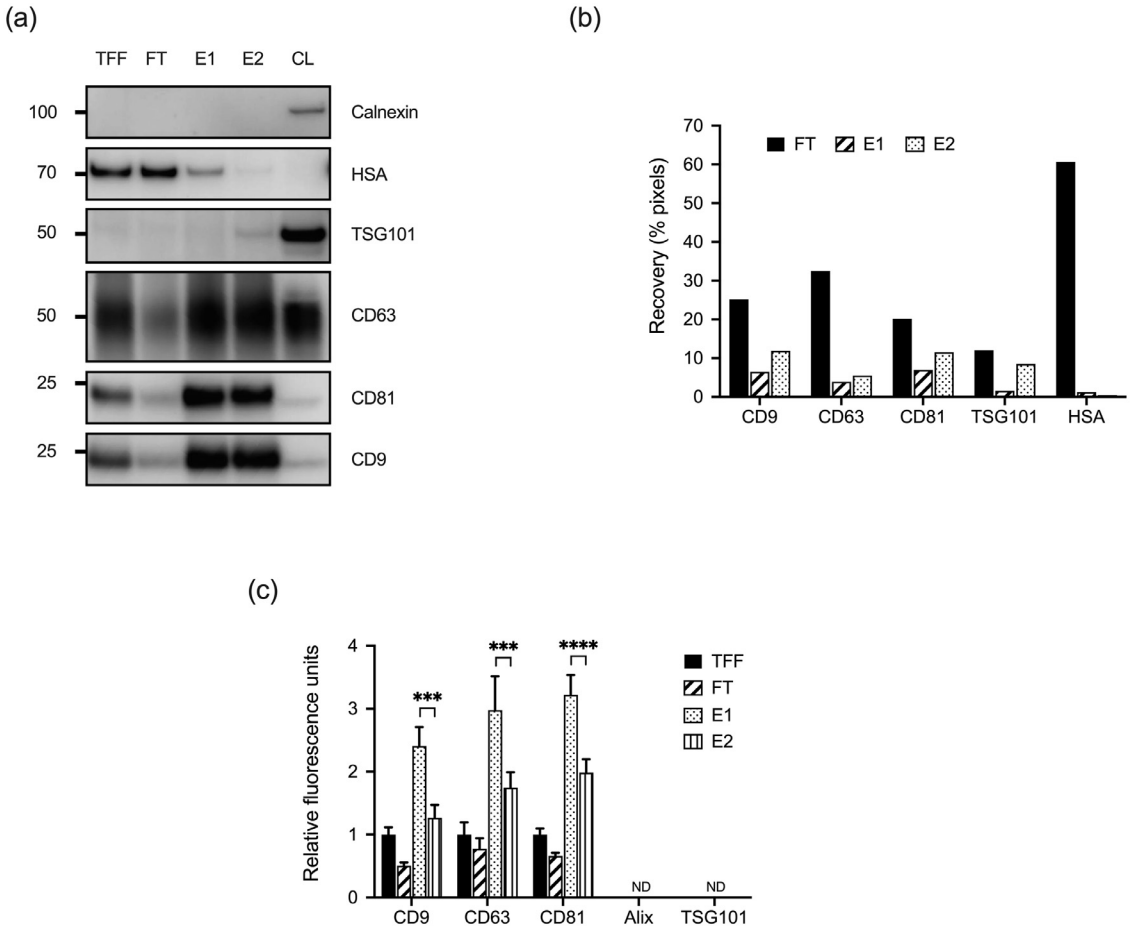

Fig. 5. Characterisation of protein markers by western blot and ELISA analysis of fractions from heparin affinity chromatography (HAC) using a step elution gradient. (a) Western blot analysis of EV markers (TSG101, CD9, CD63 and CD81) and impurity markers (Calnexin and human serum albumin, HSA). 2 ug of total protein was loaded per lane except for the anti-TSG101 blot which was loaded with 20 ug of protein per lane. (b) Recovery based on densitometry analysis of western blots (c) ELISA analysis of external EV markers (CD9, CD63 and CD81) and internal EV markers (Alix and TSG101). 1 µg of protein was incubated in each well. ELISA samples were not lysed. Error bars represent the standard deviation of technical repeats ($n = 3$). TFF: tangential flow filtration material; FT: HAC flowthrough; E1: HAC elution fraction 1; E2: HAC elution fraction 2; CL: CTX cell lysate; ND: not detected.

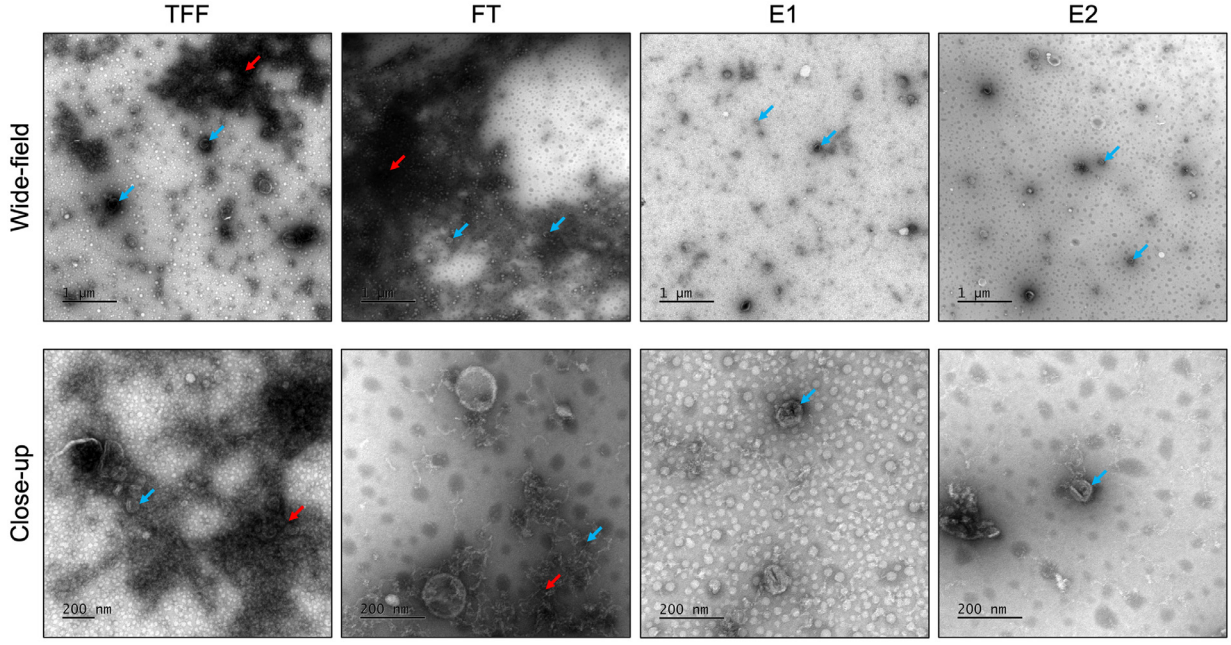

Fig. 6. Transmission electron micrographs of pooled heparin affinity chromatography (HAC), using a step elution gradient, fractions. Undiluted samples were negatively stained with 1% uranyl acetate (w/v). Blue arrows indicate examples of the characteristic concaved-disc EV structure. Red arrows indicate suspected areas of protein aggregation. TFF: tangential flow filtration material; FT: HAC flowthrough; E1: HAC elution fraction 1; E2: HAC elution fraction 2.

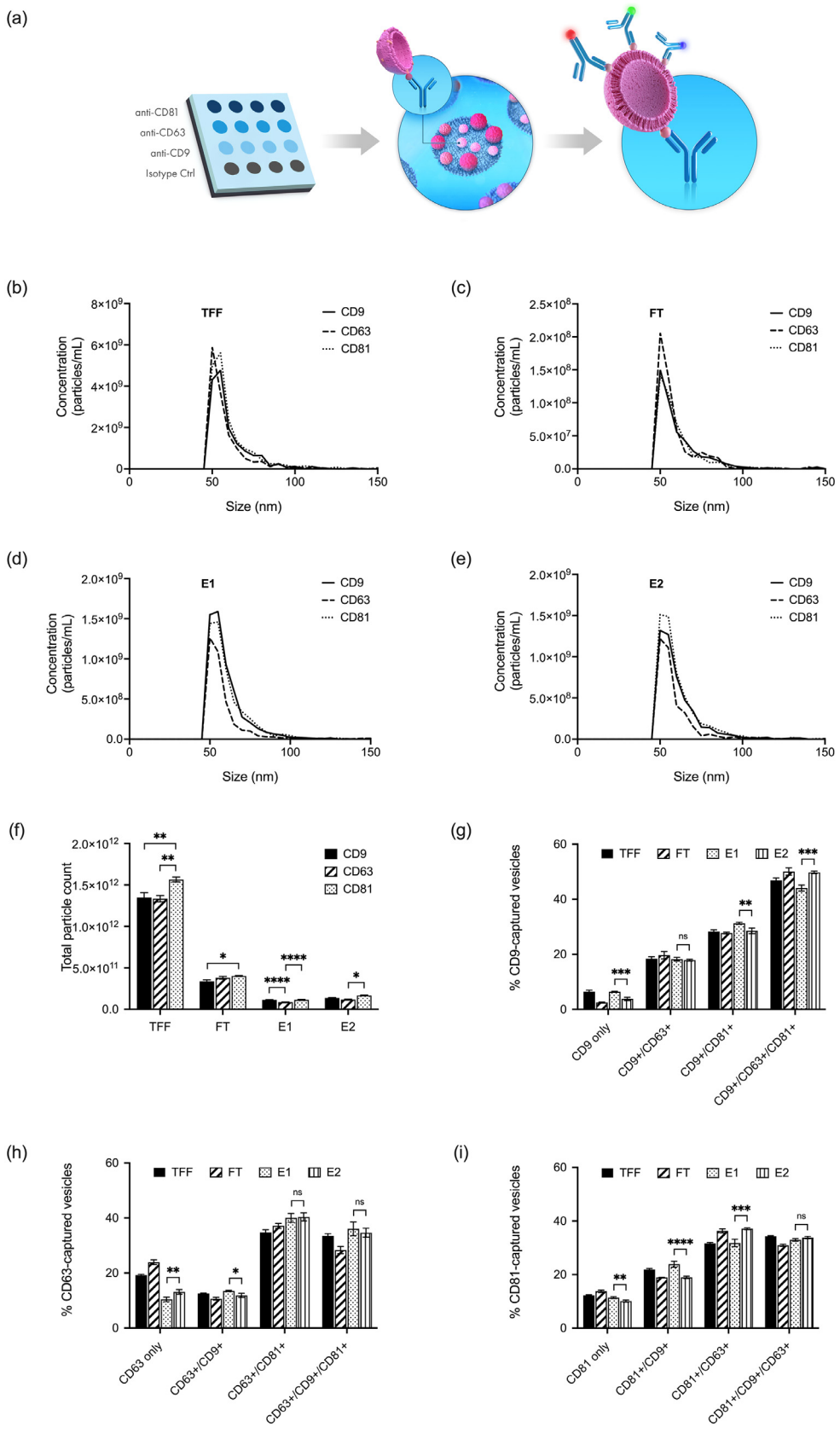

Fig. 7. ExoView platform analysis of heparin affinity chromatography (HAC), using a step elution gradient, fractions. (a) Protocol overview used with permission from NanoView Biosciences. (b-e) Marker-positive particle size distributions. (f) Total particle counts were calculated by multiplying dilution-adjusted particle counts by 50,000. (g) Colocalisation analysis of CD9-captured vesicles. (h) Colocalisation analysis of CD63-captured vesicles. (i) Colocalisation analysis of CD81-captured vesicles. Error bars represent the standard deviation of technical repeats ($n = 3$). Not significant (ns) $p > 0.05$, * $p < 0.05$, ** $p < 0.01$, *** $p < 0.001$, **** $p < 0.0001$, one-way analysis of variance. For f, ns is not shown for simplicity. For g–i, analysis of variance results are only shown between E1 and E2 for simplicity. TFF: tangential flow filtration material; FT: HAC flowthrough; E1: HAC elution fraction 1; E2: HAC elution fraction 2.

vesicles were often associated with CD63 and CD81. Only around 5% of vesicles were only CD9 positive. Whereas 40–50% of CD9-positive vesicles were also positive for one other tetraspanin and 40–50% were positive for all three markers. For CD63-captured vesicles, vesicles positive for only CD63 were more dominant in TFF material and the FT fraction. Interestingly, around 70–80% of CD63-positive vesicles were also positive for CD81. For CD81-captured vesicles, around 10% were only CD81-positive, around 20% were positive for both CD81 and CD9, around 35% were positive for CD81 and CD63, whereas around 35% were positive for all three tetraspanins, across all four samples. Analysis of variance, from technical repeats, was used to determine statistical differences in the tetraspanin phenotype between E1 and E2. The proportion of several tetraspanin phenotypes were statistically different between E1 and E2. For instance, the proportion of CD81-captured vesicles displaying two markers, CD81 and CD9, were significantly higher in E1 compared with E2.

4. Discussion

EVs continue to gain traction as future medicinal delivery platforms, diagnostic tools, and as therapeutics. However, there is not a consistent method used for EV purification by the scientific community both in the laboratory and in industry. This is due to a lack of techniques that offer sufficient purification which can also be scaled. The aim of this study was to investigate whether there is evidence of affinity between EVs and heparin and whether HAC has the potential to be used for EV purification and EV fractionation.

The affinity between heparin and EVs has previously been investigated with conflicting conclusions. Balaj et al. [15] describes the use of heparin affinity beads for EV purification supporting an interaction between heparin and EVs. Conversely, Reiter et al. [16] used HAC to bind virus-like particles to separate them from EVs which supports the absence of or low affinity between heparin and EVs. In this study, we detected EVs in both elution peaks and FT, which indicates some EV populations can bind heparin whereas another population cannot. Our results support affinity between some EVs and heparin and the strength of this affinity was used to fractionate EVs into populations that exhibited significantly different marker expressions.

EV recovery was quantified based on NTA particle data and volume-adjusted western blot densitometry data. Using the EV purification protocol (i.e., linear elution gradient) particle recovery was 68.7% compared to 39.8% using the SEC set-up. While we acknowledge that there is some uncertainty in the correlation between NTA particles and EVs, HAC resulted in a 72.6% increase in particle recovery over SEC. Based on western blot densitometry analysis, the average tetraspanin marker recovery was 26.4% (standard deviation, 12.9%) and 31.1% (standard deviation, 17.5%) for the HAC and SEC protocol respectively. We expect large standard deviations are a result of the compounding of errors by standardising pixels to fraction volumes and the semi-quantitative nature of densitometry.

As the focus of the study switched to the fractionation of EVs using the step elution gradient protocol, we increased the load volume from 0.5 mL (EV purification protocol) to 3.2 mL. We made the decision to increase the load volume to maximise the number of EVs in elution fractions to aid downstream EV analysis, at the expense of yield. We saw a reduction in particle recovery from 68.7% to 20.4% and a reduction in densitometry-based tetraspanin marker recovery from 26.4% (standard deviation, 12.9%) to 15.4% (standard deviation, 5.2%), which suggests saturation of the column. While the optimisation of column load and capacity determination was not the focus of this study, we can deduce the capacity lies between 0.5–3.2 mL of TFF material per 1 mL column. However, considering the lack of methods to directly measure EVs and the considerable variation in particles and total protein between EV production processes, and indeed batches, the reproducibility of this capacity estimate is unclear. We welcome future studies on the optimisation of HAC, which could include capacity determination and buffer/pH optimisation. One advantage of bind-elute chromatography is scalability, with manufacturing-scale columns of several hundred litres reported in the literature [24] and volumes exceeding this reported in some larger-scale industrial processes. If capacities of bead-based matrices are insufficient for application, monolith- and fibre-based matrices, which offer higher surfaces areas for EV binding, are a consideration.

The purity of EV preparations is essential for accurate research outcomes and safe and effective EV-based products. In this study, the use of HAC resulted in an average reduction of 1.93 LRV (98.8%) of protein and 1.99 LRV (99.0%) of dsDNA from TFF material. As a comparison, a typical protein A chromatography process for monoclonal antibody capture can remove 99.4% and 99.0% of host-cell proteins and DNA respectively [25]. Protein A forms a highly robust and specific interaction to monoclonal antibodies and therefore may not be the closest comparison. However, we have demonstrated HAC can result in highly pure EVs. Furthermore, we believe a transition to more rigorous measures of purification performance would be a beneficial step forward in the EV field.

It is essential the method of EV purification results in undamaged and intact EVs to preserve functional activity. This study does provide some evidence to support EVs remain undamaged following HAC. As a broad measure, ExoView size distributions (and NTA size distributions) show EVs are of an appropriate size and there are no major differences when comparing the column load material (TFF material) to elution fractions. We may expect to see a reduction in particle size from damaged EVs. Additionally, we would expect the ability of damaged EVs to be captured and counterstained using the ExoView platform to be impaired, which is not the case. Lastly, the lack of Alix and TSG101 signal in the ELISA further suggests the EV membrane remains intact, as these two markers are present within the lumen of the EVs.

The dose of EVs required for functional studies is highly dependant on the potency against the intended target, which can vary widely with each payload, EV product production, EV source and delivery method. Multiple studies have reported EV doses for murine studies in the range of 10^9 to 10^{11} particles and 10 to 150 µg of total protein [26]. The linear elution gradient HAC protocol used in this study resulted in 8.45×10^{10} total particles and 189 µg of total protein. Therefore, the EV recovery from columns used in this publication could reasonably be expected to provide sufficient recovery for a murine *in vivo* study; but this would ultimately be dictated by the potency of the payload of interest. It is also possible to scale this approach up for larger-scale studies or studies in larger model organisms, as described above.

Several techniques have been described to separate EVs into subpopulations. The most established techniques separate EVs based on size and include differential ultracentrifugation and density separation [27] and asymmetrical-flow field-flow fractionation [28]. In this study, we expect HAC is separating EVs into three populations based on their affinity to heparin, where EVs with no affinity to heparin remain in the flowthrough (FT); EVs with some affinity to heparin elute at 0.2 M NaCl (E1) and EVs with higher affinity to heparin elute at 0.4 M NaCl (E2). This difference in affinity to heparin could be caused by variable expression of heparin ligands on the EV membrane, the presence of different heparin ligands on the EV membrane or the association of EVs with different bound heparin ligands. The boundary between what are unique EV subpopulations and just heterogeneity in marker expression is not well-defined in the field. Therefore, we cannot definitively conclude the separation of ‘true’ EV subpopulations but populations

with differences in tetraspanin phenotype and TSG101 expression. Further investigation into the EVs in each population may lead to new insights into the mode of interaction and may identify compositional or functional differences, other than the differences shown in this study.

Overall, we have shown there is evidence of affinity between EVs and heparin. While the mechanism of interaction between heparin and EVs is unknown, we can deduce the dominant mechanism of interaction is pseudo-affinity. It is less likely heparin is acting as a cation exchanger because the EV surface holds a net negative charge [29], which has been exploited with anion exchange-based EV capture [30,31]. However, a better understanding of this interaction is needed before HAC can be adopted for EV-based applications. This could lead to the development of custom chromatography ligands with altered heparin structures with better affinity and specificity for EVs and more optimised chromatography protocols. This will also allow us to better understand what impurity proteins are binding to heparin, which we expect is due to its broad ligand binding properties. With this understanding, HAC could be further developed as a second purification or polishing step as explored in this study. Alternatively, it could potentially be optimised for EV capture in more crude preparations such as cell culture medium. However, the broad binding properties of heparin may limit this application. In terms of the application of HAC for EV fractionation, a more detailed proteomic analysis of elution peaks, with a focus on known heparin-binding proteins, is needed to establish if these protocols are truly isolating EV subpopulations with differing molecular profiles.

5. Conclusions

HAC resulted in highly pure EVs in elution fractions and we found EV recovery was higher than when a standard SEC protocol was used. Our results add to the evidence supporting the application of HAC for EV purification. In addition, we have proposed a novel application of HAC for EV fractionation. The implications of both a direct EV binder and potentially an alternative method to separation EV subpopulations are potentially far-reaching both for advancing our understanding of EVs and for improving the manufacture of EV-based products. While we cannot conclude there is a direct interaction between heparin and EVs, this study does support that hypothesis. Therefore, we believe further investigation into this interaction by the scientific community is justified moving forward.

Funding

This work was supported by a 4-year EPSRC EngD programme at University College London that was sponsored by ReNeuron (grant code: EP/L01520X/1) and by an Industrial Fellowship from the Royal Commission for the Exhibition of 1851.

Declaration of competing interest

Authors, Samantha Thomas and Paul Hole, are currently employees at ReNeuron who provided the EV TFF material for this study. ReNeuron also partially funded the work in this study.

CRediT authorship contribution statement

Benjamin Barnes: Conceptualization, Data curation, Formal analysis, Funding acquisition, Investigation, Methodology, Project administration, Visualization, Writing – original draft, Writing – review & editing. **Thomas Caws:** Methodology, Resources. **Samantha Thomas:** Methodology, Resources, Supervision, Writing – review & editing. **Alex P. Shephard:** Investigation, Data curation, Formal analysis, Writing – review & editing. **Randolph Corteling:** Conceptualization, Funding acquisition, Resources, Supervision. **Paul Hole:** Supervision, Writing – review & editing. **Daniel G. Bracewell:** Conceptualization, Funding acquisition, Resources, Supervision, Writing – review & editing.

Acknowledgements

We thank Mark Turmaine (UCL Division of Biosciences) for providing technical support with the TEM imaging. We also thank Philip Koon (ReNeuron) for his support with various aspects of extracellular vesicle production and analysis.

Appendix

Fig. A1, Fig. A2, Fig. A3, Fig. A4

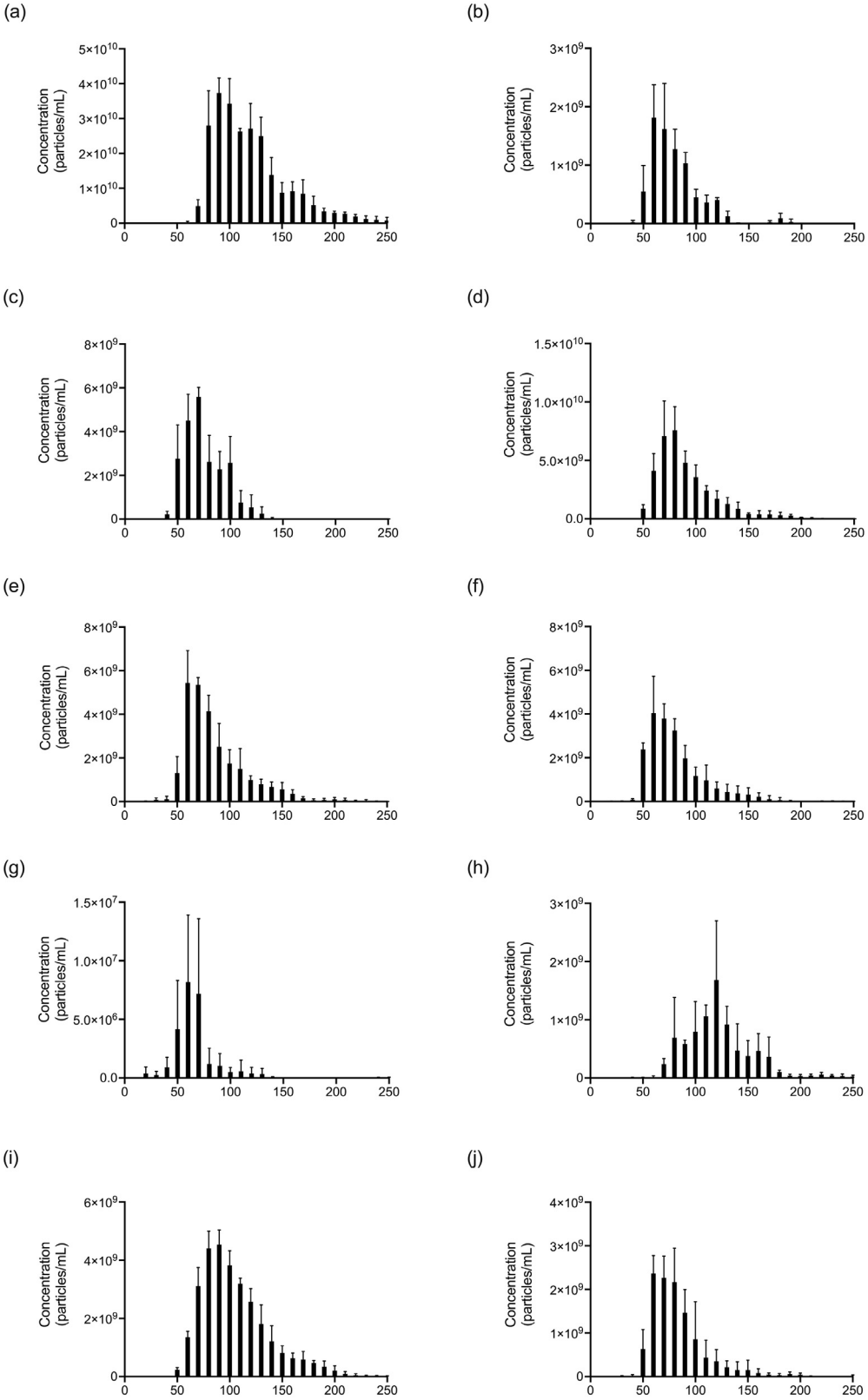

Fig. A1. Particle size distributions for tangential flow filtration material (TFF), heparin affinity chromatography (HAC), using a linear elution gradient, fractions and size-exclusion chromatography fractions (SEC). (a) TFF. (b) H1. (c) H2. (d) H3. (e) H4. (f) H5. (g) S1. (h) S2. (i) S3. (j) S4. Error bars represent the standard deviation of technical repeats ($n = 3$). H1–H5: HAC fractions 1–5; S1–S4: SEC fractions 1–4.

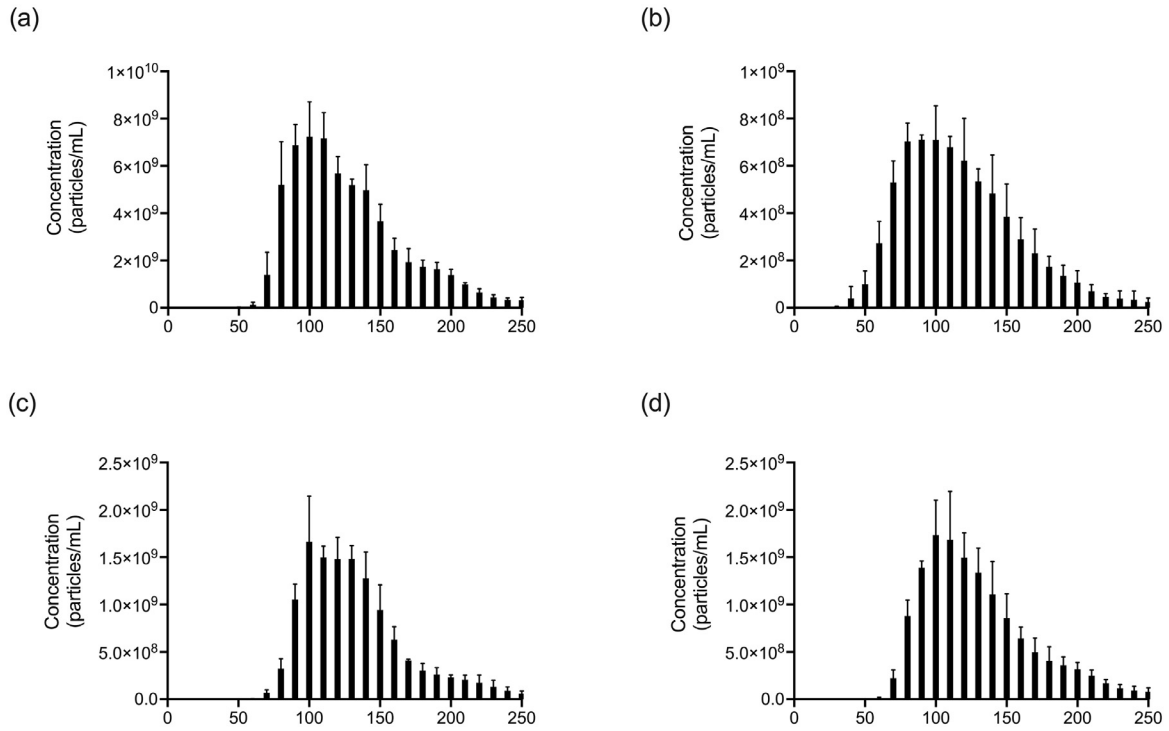

Fig. A2. Fig. A1. Particle size distributions for tangential flow filtration material (TFF) and heparin affinity chromatography (HAC), using a step elution gradient, fractions. (a) TFF. (b) HAC flowthrough. (c) HAC elution fraction 1. (d) HAC elution fraction 2. Error bars represent the standard deviation of technical repeats ($n = 3$).

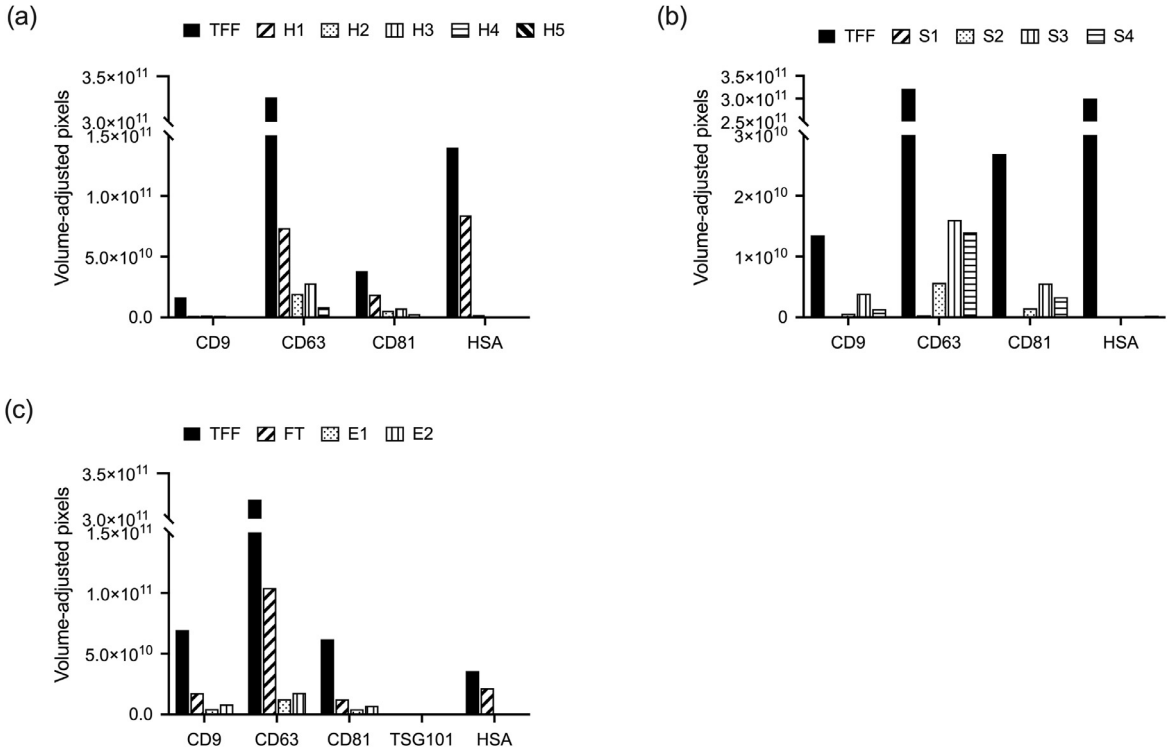

Fig. A3. Volume-adjusted pixel counts based on western blots. (a) Heparin affinity chromatography (HAC) using a linear elution gradient based on Fig. 2g. (b) Size-exclusion chromatography (SEC) based on Fig. 3g. HAC using a step elution gradient based on Fig. 5a. TFF: tangential flow filtration material; H1–H5: HAC, using a linear elution gradient, fractions 1–5; S1–S4: SEC fractions 1–4; FT: HAC, using a step elution gradient, flowthrough; E1: HAC, using a step elution gradient elution, fraction 1; E2: HAC, using a step elution gradient, elution fraction 2.

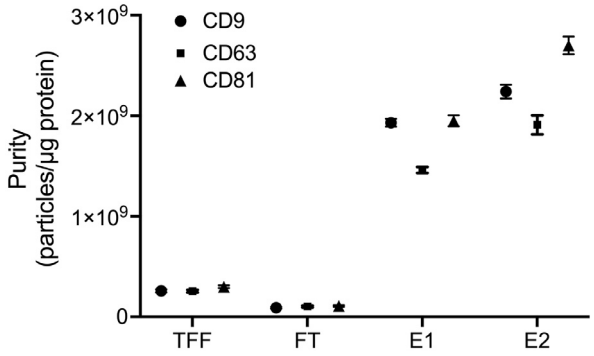

Fig. A4. ExoView-based purity of tangential flow filtration material (TFF) and heparin affinity chromatography (HAC), using a step elution gradient, fractions. Purity was calculated from tetraspanin-positive particle counts. Error bars represent the standard deviation of technical repeats ($n = 3$). FT: HAC flowthrough; E1: HAC elution fraction 1; E2: HAC elution fraction 2.

References

[1] I.L. Colao, R. Corteling, D. Bracewell, I. Wall, Manufacturing exosomes: a promising therapeutic platform, Trends Mol. Med. (2018) 1–15, doi:10.1016/j.molmed.2018.01.006.

[2] C.B. Reimer, R.S. Baker, R.M. vanFrank, T.E. Newlin, G.B. Cline, N.G. Anderson, Purification of large quantities of influenza virus by density gradient centrifugation, J. Virol. (1967) 1, doi:10.1128/jvi.1.6.1207-1216.1967.

[3] R. Wei, L. Zhao, G. Kong, X. Liu, S. Zhu, S. Zhang, L. Min, Combination of size-exclusion chromatography and ultracentrifugation improves the proteomic profiling of plasma-derived small extracellular vesicles, Biol. Proced. Online. (2020) 22, doi:10.1186/s12575-020-00125-5.

[4] W. Nakai, T. Yoshida, D. Diez, Y. Miyatake, T. Nishibu, N. Imawaka, K. Naruse, Y. Sadamura, R. Hanayama, A novel affinity-based method for the isolation of highly purified extracellular vesicles, Sci. Rep. 6 (2016) 1–11, doi:10.1038/srep33935.

[5] E.E. Burkova, P.S. Dmitrenok, D.V. Bulgakov, V.V. Vlassov, E.I. Ryabchikova, G.A. Nevinsky, Exosomes from human placenta purified by affinity chromatography on sepharose bearing immobilized antibodies against CD81 tetraspanin contain many peptides and small proteins, IUBMB Life 70 (2018), doi:10.1002/iub.1928.

[6] D.K. Jeppesen, A.M. Fenix, J.L. Franklin, J.N. Higginbotham, Q. Zhang, L.J. Zimmerman, D.C. Liebler, J. Ping, Q. Liu, R. Evans, W.H. Fissell, J.G. Patton, L.H. Rome, D.T. Burnette, R.J. Coffey, Reassessment of exosome composition, Cell (2019) 177, doi:10.1016/j.cell.2019.02.029.

[7] D. Guan, Z. Chen, Challenges and recent advances in affinity purification of tag-free proteins, Biotechnol. Lett. (2014) 36, doi:10.1007/s10529-014-1509-2.

[8] A.A. Navarro Del Cañizo, M. Mazza, R. Bellinzoni, O. Cascone, Foot and mouth disease virus concentration and purification by affinity chromatography, Appl. Biochem. Biotechnol. - Part A Enzym. Eng. Biotechnol. (1996) 61, doi:10.1007/bf02787811.

[9] A. Staby, M.B. Sand, R.G. Hansen, J.H. Jacobsen, L.A. Andersen, M. Gerstenberg, U.K. Bruus, I.H. Jensen, Comparison of chromatographic ion-exchange resins: IV. Strong and weak cation-exchange resins and heparin resins, J. Chromatogr. A (2005), doi:10.1016/j.chroma.2004.11.094.

[10] A.K. Powell, E.A. Yates, D.G. Fernig, J.E. Turnbull, Interactions of heparin/heparan sulfate with proteins: appraisal of structural factors and experimental approaches, Glycobiology (2004) 14, doi:10.1093/glycob/cwh051.

[11] P.M. Kraemer, Heparan Sulfates of Cultured Cells. I. Membrane-Associated and Cell-Sap Species in Chinese Hamster Cells, Biochemistry (1971) 10, doi:10.1021/bi00784a026.

[12] P.M. Kraemer, Heparan sulfates of cultured cells. II. Acid-soluble and -precipitable species of different cell lines, Biochemistry (1971) 10, doi:10.1021/bi00784a027.

[13] M. Bernfield, M. Götte, P.W. Park, O. Reizes, M.L. Fitzgerald, J. Lincecum, M. Zako, Functions of cell surface heparan sulfate proteoglycans, Annu. Rev. Biochem. (1999) 68, doi:10.1146/annurev.biochem.68.1.729.

[14] H.C. Christianson, K.J. Svensson, T.H. Van Kuppevelt, J.P. Li, M. Belting, Cancer cell exosomes depend on cell-surface heparan sulfate proteoglycans for their internalization and functional activity, Proc. Natl. Acad. Sci. U. S. A. 110 (2013) 17380–17385, doi:10.1073/pnas.1304266110.

[15] L. Balaj, N.A. Atai, W. Chen, D. Mu, B.A. Tannous, X.O. Breakefield, J. Skog, C.A. Maguire, Heparin affinity purification of extracellular vesicles, Sci. Rep. 5 (2015) 1–15, doi:10.1038/srep10266.

[16] K. Reiter, P.P. Aguilar, V. Wetter, P. Steppert, A. Tover, A. Jungbauer, Separation of virus-like particles and extracellular vesicles by flow-through and heparin affinity chromatography, J. Chromatogr. A. 1588 (2019) 77–84, doi:10.1016/j.chroma.2018.12.035.

[17] N.A. Atai, L. Balaj, H. Van Veen, X.O. Breakefield, P.A. Jarzyna, C.J.F. Van Noorden, J. Skog, C.A. Maguire, Heparin blocks transfer of extracellular vesicles between donor and recipient cells, J. Neurooncol. (2013) 115, doi:10.1007/s11060-013-1235-y.

[18] K. Pollock, P. Stroemer, S. Patel, L. Stevanato, A. Hope, E. Miljan, Z. Dong, H. Hodges, J. Price, J.D. Sinden, A conditionally immortal clonal stem cell line from human cortical neuroepithelium for the treatment of ischemic stroke, Exp. Neurol. 199 (2006) 143–155, doi:10.1016/j.expneurol.2005.12.011.

[19] S.A. Gazze, S.J. Thomas, J. Garcia-Parra, D.W. James, P. Rees, V. Marsh-Durban, R. Corteling, D. Gonzalez, R.S. Conlan, L.W. Francis, High content, quantitative AFM analysis of the scalable biomechanical properties of extracellular vesicles, Nanoscale (2021) 13, doi:10.1039/d0nr09235e.

[20] J.L. Welton, P. Brennan, M. Gurney, J.P. Webber, L.K. Spary, D.G. Carton, J.M. Falcón-Pérez, S.P. Walton, M.D. Mason, Z. Tabi, A. Clayton, Proteomics analysis of vesicles isolated from plasma and urine of prostate cancer patients using a multiplex, aptamer-based protein array, J. Extracell. Vesicles. 5 (2016), doi:10.3402/jev.v5.31209.

[21] J.L. Welton, S. Loveless, T. Stone, C. von Ruhland, N.P. Robertson, A. Clayton, Cerebrospinal fluid extracellular vesicle enrichment for protein biomarker discovery in neurological disease; multiple sclerosis, J. Extracell. Vesicles. (2017) 6, doi:10.1080/20013078.2017.1369805.

[22] J. Webber, T.C. Stone, E. Katilius, B.C. Smith, B. Gordon, M.D. Mason, Z. Tabi, I.A. Brewis, A. Clayton, Proteomics analysis of cancer exosomes using a novel modified aptamer-based array (somascantm) platform, Mol. Cell. Proteomics. (2014) 13, doi:10.1074/mcp.M113.032136.

[23] C. Théry, K.W. Witwer, E. Aikawa, M.J. Alcaraz, J.D. Anderson, R. Andriantsitohaina, A. Antoniou, T. Arab, F. Archer, G.K. Atkin-Smith, D.C. Ayre, J.M. Bach, D. Bachurski, H. Baharvand, L. Balaj, S. Baldacchino, N.N. Bauer, A.A. Baxter, M. Bebawy, C. Beckham, A. Bedina Zavec, A. Benmoussa, A.C. Berardi, P. Bergese, E. Bielska, C. Blenkiron, S. Bobis-Wozowicz, E. Boilard, W. Boireau, A. Bongiovanni, F.E. Borràs, S. Bosch, C.M. Boulanger, X. Breakefield, A.M. Breglio, M. Brennan, D.R. Brigstock, A. Brisson, M.L.D. Broekman, J.F. Bromberg, P. Bryl-Górecka, S. Buch, A.H. Buck, D. Burger, S. Busatto, D. Buschmann, B. Bussolati, E.I. Buzás, J.B. Byrd, G. Camussi, D.R.F. Carter, S. Caruso, L.W. Chamley, Y.T. Chang, A.D. Chaudhuri, C. Chen, S. Chen, L. Cheng, A.R. Chin, A. Clayton, S.P. Clerici, A. Cocks, E. Cocucci, R.J. Coffey, A. Cordeiro-da-Silva, Y. Couch, F.A.W. Coumans, B. Coyle, R. Crescitelli, M.F. Criado, C. D'Souza-Schorey, S. Das, P. de Candia, E.F. De Santana, O. De Wever, H.A. del Portillo, T. Demaret, S. Deville, A. Devitt, B. Dhondt, D. Di Vizio, L.C. Dieterich, V. Dolo, A.P. Dominguez Rubio, M. Dominici, M.R. Dourado, T.A.P. Driedonks, F.V. Duarte, H.M. Duncan, R.M. Eichenberger, K. Ekström, S. EL Andaloussi, C. Elie-Caille, U. Erdbrügger, J.M. Falcón-Pérez, F. Fatima, J.E. Fish, M. Flores-Bellver, A. Försönits, A. Frelet-Barrand, F. Fricke, G. Fuhrmann, S. Gabrielsson, A. Gámez-Valero, C. Gardiner, K. Gärtner, R. Gaudin, Y.S. Gho, B. Giebel, C. Gilbert, M. Gimona, I. Giusti, D.C.I. Goberdhan, A. Görgens, S.M. Gorski, D.W. Greening, J.C. Gross, A. Gualerzi, G.N. Gupta, D. Gustafson, A. Handberg, R.A. Haraszti, P. Harrison, H. Hegyesi, A. Hendrix, A.F. Hill, F.H. Hochberg, K.F. Hoffmann, B. Holder, H. Holthofer, B. Hosseinkhani, G. Hu, Y. Huang, V. Huber, S. Hunt, A.G.E. Ibrahim, T. Ikezu, J.M. Inal, M. Isin, A. Ivanova, H.K. Jackson, S. Jacobsen, S.M. Jay, M. Jayachandran, G. Jenster, L. Jiang, S.M. Johnson, J.C. Jones, A. Jong, T. Jovanovic-Talisman, S. Jung, R. Kalluri, S. ichi Kano, S. Kaur, Y. Kawamura, E.T. Keller, D. Khamari, E. Khomyakova, A. Khvorova, P. Kierulf, K.P. Kim, T. Kislinger, M. Klingeborn, D.J. Klinke, M. Kornek, M.M. Kosanović, Á.F. Kovács, E.M. Krämer-Albers, S. Krasemann, M. Krause, I.V. Kurochkin, G.D. Kusuma, S. Kuypers, S. Laitinen, S.M. Langevin, L.R. Languino, J. Lannigan, C. Lässer, L.C. Laurent, G. Lavieu, E. Lázaro-Ibáñez, S.Le Lay, M.S. Lee, Y.X.F. Lee, D.S. Lemos, M. Lenassi, A. Leszczynska, I.T.S. Li, K. Liao, S.F. Libregts, E. Ligeti, R. Lim, S.K. Lim, A. Linē, K. Linnemannstöns, A. Llorente, C.A. Lombard, M.J. Lorenowicz, Á.M. Lörincz, J. Lötvall, J. Lovett, M.C. Lowry, X. Loyer, Q. Lu, B. Lukomska, T.R. Lunavat, S.L.N. Maas, H. Malhi, A. Marcilla, J. Mariani, J. Mariscal, E.S. Martens-Uzunova, L. Martin-Jaular, M.C. Martinez, V.R. Martins, M. Mathieu, S. Mathivanan, M. Maugeri, L.K. McGinnis, M.J. McVey, D.G. Meckes, K.L. Meehan, I. Mertens, V.R. Minciacchi, A. Möller, M. Møller Jørgensen, A. Morales-Kastresana, J. Morhayim, F. Mullier, M. Muraca, L. Musante, V. Mussack, D.C. Muth, K.H. Myburgh, T. Najrana, M. Nawaz, I. Nazarenko, P. Nejsum, C. Neri, T. Neri, R. Nieuwland, L. Nimrichter, J.P. Nolan, E.N.M. Nolte-'t Hoen, N. Noren Hooten, L O'Driscoll, T. O'Grady, A. O'Loghlen, T. Ochiya, M. Olivier, A. Ortiz, L.A. Ortiz, X. Osteikoetxea, O. Ostegaard, M. Ostrowski, J. Park, D.M. Pegtel, H. Peinado, F. Perut, M.W. Pfaffl, D.G. Phinney, B.C.H. Pieters, R.C. Pink, D.S. Pisetsky, E. Pogge von Strandmann, I. Polakovicova, I.K.H. Poon, B.H. Powell, I. Prada, L. Pulliam, P. Quesenberry, A. Radeghieri, R.L. Raffai, S. Raimondo, J. Rak, M.I. Ramirez, G. Raposo, M.S. Rayyan, N. Regev-Rudzki, F.L. Ricklefs, P.D. Robbins, D.D. Roberts, S.C. Rodrigues, E. Rohde, S. Rome, K.M.A. Rouschop, A. Rughetti, A.E. Russell, P. Saá, S. Sahoo, E. Salas-Huenuleo, C. Sánchez, J.A. Saugstad, M.J. Saul, R.M. Schiffelers, R. Schneider, T.H. Schøyen, A. Scott, E. Shahaj, S. Sharma, O. Shatnyeva, F. Shekari, G.V. Shelke, A.K. Shetty, K. Shiba, P.R.M. Siljander, A.M. Silva, A. Skowronek, O.L. Snyder, R.P. Soares, B.W. Sódar, C. Soekmadji, J. Sotillo, P.D. Stahl, W. Stoorvogel, S.L. Stott, E.F. Strasser, S. Swift, H. Tahara, M. Tewari, K. Timms, S. Tiwari, R. Tixeira, M. Tkach, W.S. Toh, R. Tomasini, A.C. Torrecilhas, J.P. Tosar, V. Toxavidis, L. Urbanelli, P. Vader, B.W.M. van Balkom, S.G. van der Grein, J. Van Deun, M.J.C. van Herwijnen, K. Van Keuren-Jensen, G. van Niel, M.E. van Royen, A.J. van Wijnen, M.H. Vasconcelos, I.J. Vechetti, T.D. Veit, L.J. Vella, É. Velot, F.J. Verweij, B. Vestad, J.L. Viñas, T. Visnovitz, K.V. Vukman, J. Wahlgren, D.C. Watson, M.H.M. Wauben, A. Weaver, J.P. Webber, V. Weber, A.M. Wehman, D.J. Weiss, J.A. Welsh, S. Wendt, A.M. Wheelock, Z. Wiener, L. Witte, J. Wolfram, A. Xagorari, P. Xander, J. Xu, X. Yan, M. Yáñez-Mó, H. Yin, Y. Yuana, V. Zappulli, J. Zarubova, V. Žėkas, J. ye Zhang, Z. Zhao, L. Zheng, A.R. Zheutlin, A.M. Zickler,

P. Zimmermann, A.M. Zivkovic, D. Zocco, E.K. Zuba-Surma, Minimal information for studies of extracellular vesicles 2018 (MISEV2018): a position statement of the international society for extracellular vesicles and update of the MISEV2014 guidelines, J. Extracell. Vesicles. 7 (2018), doi:10.1080/20013078.2018.1535750.

[24] S. Aldington, J. Bonnerjea, Scale-up of monoclonal antibody purification processes, J. Chromatogr. B Anal. Technol. Biomed. Life Sci. 848 (2007), doi:10.1016/j.jchromb.2006.11.032.

[25] R.L. Fahrner, D.H. Whitney, M. Vanderlaan, G.S. Blank, Performance comparison of Protein A affinity-chromatography sorbents for purifying recombinant monoclonal antibodies, Biotechnol. Appl. Biochem. (1999) 30, doi:10.1111/j.1470-8744.1999.tb00902.x.

[26] D. Gupta, A.M. Zickler, S. El Andaloussi, Dosing extracellular vesicles, Adv. Drug Deliv. Rev. (2021) 178, doi:10.1016/j.addr.2021.113961.

[27] R. Crescitelli, C. Lässer, J. Lötvall, Isolation and characterization of extracellular vesicle subpopulations from tissues, Nat. Protoc. (2021) 16, doi:10.1038/s41596-020-00466-1.

[28] H. Zhang, D. Freitas, H.S. Kim, K. Fabijanic, Z. Li, H. Chen, M.T. Mark, H. Molina, A.B. Martin, L. Bojmar, J. Fang, S. Rampersaud, A. Hoshino, I. Matei, C.M. Kenific, M. Nakajima, A.P. Mutvei, P. Sansone, W. Buehring, H. Wang, J.P. Jimenez, L. Cohen-Gould, N. Paknejad, M. Brendel, K. Manova-Todorova, A. Magalhães, J.A. Ferreira, H. Osório, A.M. Silva, A. Massey, J.R. Cubillos-Ruiz, G. Galletti, P. Giannakakou, A.M. Cuervo, J. Blenis, R. Schwartz, M.S. Brady, H. Peinado, J. Bromberg, H. Matsui, C.A. Reis, D. Lyden , Identification of distinct nanoparticles and subsets of extracellular vesicles by asymmetric flow field-flow fractionation, Nat. Cell Biol. 20 (2018) 332–343, doi:10.1038/s41556-018-0040-4.

[29] M.C. Deregibus, F. Figliolini, S. D'Antico, P.M. Manzini, C. Pasquino, M. De Lena, C. Tetta, M.F. Brizzi, G. Camussi, Charge-based precipitation of extracellular vesicles, Int. J. Mol. Med. (2016) 38, doi:10.3892/ijmm.2016.2759.

[30] N. Heath, L. Grant, T.M. De Oliveira, R. Rowlinson, X. Osteikoetxea, N. Dekker, R. Overman, Rapid isolation and enrichment of extracellular vesicle preparations using anion exchange chromatography, Sci. Rep. 8 (2018) 1–12, doi:10.1038/s41598-018-24163-y.

[31] M. Kosanović, B. Milutinović, S. Goč, N. Mitić, M. Janković, Ion-exchange chromatography purification of extracellular vesicles, Biotechniques (2017) 63, doi:10.2144/000114575.

[32] B.C. Nelson, S. Maragh, I.C. Ghiran, J.C. Jones, P.C. Derose, E. Elsheikh, W.N. Vreeland, L. Wang, Measurement and standardization challenges for extracellular vesicle therapeutic delivery vectors, Nanomedicine (2020) 15, doi:10.2217/nnm-2020-0206.

[33] R.P. McNamara, D.P. Dittmer, Modern techniques for the isolation of extracellular vesicles and viruses, J. Neuroimmune Pharmacol. 15 (2020), doi:10.1007/s11481-019-09874-x.